Bioresource Technology 447 (2026) 134250

Contents lists available at ScienceDirect

Bioresource Technology

journal homepage: www.elsevier.com/locate/biortech

Redox-active antioxidants enable highly stable bio-electrochemical systems

Wei Chen [a,b], Rui Bai [b,c], Biyi Zhao [a,b], Xudong Zhou [c], Feng Zhao [b,c,*], Yong Xiao [a,b,*]

[a] State Key Laboratory of Regional and Urban Ecology, Institute of Urban Environment, Chinese Academy of Sciences, Xiamen 361021, China
[b] University of Chinese Academy of Sciences, Beijing 100049, China
[c] State Key Laboratory of Advanced Environmental Technology, Institute of Urban Environment, Chinese Academy of Sciences, Xiamen 361021, China

HIGHLIGHTS

- DFT and electrochemical analyses demonstrate that fraxetin acts as an electron shuttle in oxygen-saturated conditions.
- Upon oxygen exposure, FMN-mediated current falls by ~75%, whereas fraxetin-mediated current decreases by only ~18%.
- Even at DO > 4 mg L^{-1}, fraxetin boosts current production by *Shewanella oneidensis* MR-1 by ~8-fold.
- The mechanism of fraxetin-mediated EET in *S. oneidensis* MR-1 at DO > 4 mg L^{-1} is elucidated.

GRAPHICAL ABSTRACT

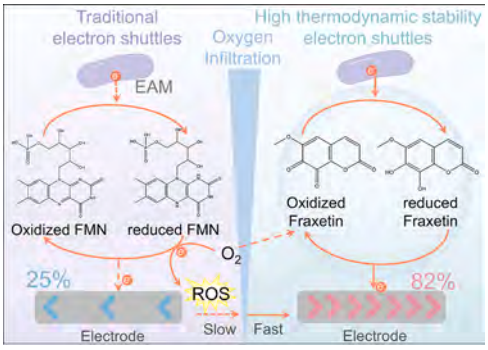

ARTICLE INFO

Keywords:
Electron shuttles
Antioxidants
Bio-electrochemical systems
Shewanella oneidensis MR-1
Oxygen infiltration

ABSTRACT

Efficient interfacial electron transfer between electroactive microorganisms and electrodes underpins bio-electrochemical systems for energy, environmental, biosensors, and bioelectronic applications. Yet oxygen infiltration, unavoidable under practical conditions, and severely impairs performance. Here, we propose a strategy where plant-sourced antioxidants, such as fraxetin, with high thermodynamic stability are employed as electron shuttles. Electrochemical analysis and density functional theory revealed that fraxetin, unlike flavin mononucleotide, resists oxygen oxidation and sustains electron transfer under saturated dissolved oxygen conditions. Additionally, oxygen infiltration caused a 75% decrease in the current generated by *Shewanella oneidensis* MR-1 mediated by flavin mononucleotide, whereas the current mediated by fraxetin only decreased by 18%. This approach provided a fundamentally different and more practical solution than physical oxygen-exclusion methods, oxygen-tolerant ESs as a robust and versatile avenue to maintain efficient interfacial electron transfer in bio-electrochemical systems under actual environments.

* Corresponding authors at: Institute of Urban Environment, Chinese Academy of Sciences, Xiamen 361021, China
E-mail addresses: fzhao@iue.ac.cn (F. Zhao), yxiao@iue.ac.cn (Y. Xiao).

https://doi.org/10.1016/j.biortech.2026.134250
Received 30 October 2025; Received in revised form 9 January 2026; Accepted 17 February 2026
Available online 17 February 2026

1. Introduction

The interfacial electron transfer between electroactive microorganisms (EAMs) and electrodes forms the foundation of bio-electrochemical systems (BESs) (Xiao et al., 2017; Zhang et al., 2024a), which show broad potential in wastewater treatment (Yan et al., 2018), energy generation (Zhang et al., 2024b), environmental monitoring (Li et al., 2025), and medical diagnostics (Aiyer & Doyle, 2022). Representative applications include microbial fuel cells that recover electricity from organic waste (Cao et al., 2021), microbial electrosynthesis that converts carbon dioxide into value-added organics (Xie et al., 2023), as well as biosensors (Atkinson et al., 2022) and wearable diagnostic devices (Choi, 2022). The efficient operation of these systems is highly dependent on maintaining anoxic conditions (Logan et al., 2019). EAMs transfer intracellular metabolic electrons to electrodes via extracellular electron transfer (EET), which occurs through two primary pathways: direct contact mediated by outer-membrane *c*-type cytochromes and indirect contact facilitated by soluble electron shuttles (ESs) (Shi et al., 2016). Among these, ESs mediated EET is particularly crucial (Kundu et al., 2025; Light et al., 2018; Okamoto et al., 2013); accounting for up to 80% of current (Marsili et al., 2008).

However, the inevitable infiltration of environmental oxygen during operation poses a significant challenge. Oxygen interferes with the interfacial electron transfer process, thereby inhibiting system efficiency and limiting their practical applications (Harnisch et al., 2024; Logan et al., 2019). Most crucially, most ESs are highly susceptible to oxygen, with their shuttling capacity diminished by direct oxidation (Khan et al., 2012; Ma et al., 2025; Price-Whelan et al., 2006), while the concomitant generation of reactive oxygen species (ROS) further damages EAMs and compromises BESs efficiency. Engineering strategies, such as optimizing reactor/electrode configurations or introducing ion-exchange membranes as physical barriers, have been explored to mitigate oxygen infiltration (Amirdehi et al., 2020; Choi & Chae, 2013; Li et al., 2023; Yang et al., 2019; Yoon et al., 2018). However, these physical-barrier-based approaches often suffer from limited long-term stability and generality and, more critically, largely overlook the chemical stability of ESs. Enhancing the chemical stability of ESs may provide a fundamental solution to the oxygen infiltration hindrance of interfacial electron transfer, a direction that remains scarcely explored.

Interestingly, plants have evolved highly efficient antioxidant defense systems to survive in oxygen rich environments (Mittler et al., 2022). At their core are small molecules with both strong chemical stability and redox activity, which eliminate ROS and maintain cellular redox homeostasis (Mittler et al., 2022; Wang et al., 2025). The essence of ROS scavenging is that reductive antioxidants reduce oxidative ROS, representing electron transfer from antioxidants to ROS under oxic conditions (Li et al., 2020; Shahidi & Ambigaipalan, 2015). This process bears strong mechanistic resemblance to the reversible electron exchanging between microbes and electrodes in BESs. Inspired by these parallels, we investigated the potential of natural antioxidants to mitigate the impact of oxygen diffusion and sustain efficient interfacial electron transfer, providing a new and generalizable concept for stabilizing BES performance.

Here, we combined electrochemical analysis with density functional theory (DFT) calculations to dissect, at the molecular level, the oxygen stability and redox thermodynamics of the classical ES flavin mononucleotide (FMN) (Light et al., 2018; Marsili et al., 2008; Okamoto et al., 2013) and the natural antioxidant fraxetin with redox activity (McRose et al., 2023; Medina et al., 2014). We further evaluated how oxygen permeation affects the efficiency of FMN or fraxetin mediated interfacial electron transfer between *Shewanella oneidensis* MR-1 (a model EAM strain widely used in BESs studies) (Lin et al., 2021; Xiao et al., 2021; Yang et al., 2020) and electrodes. Moreover, transcriptomic and genetic analyses were conducted to elucidate the molecular mechanism by which fraxetin promotes EET of *S. oneidensis* MR-1 under oxic conditions. Together, this study provides molecular-level evidence and strategic insights into sustaining efficient EAMs–electrodes interfacial electron transfer under oxygen intrusion, and offers a generalizable framework for the selection of ESs tailored for oxygen infiltration environments.

2. Materials and methods

2.1. Materials

Ammonium chloride (NH_4Cl), dipotassium hydrogen phosphate (K_2HPO_4), sodium chloride (NaCl), and sodium lactate ($C_3H_5NaO_3$) were purchased from Sinopharm Chemical Reagent Co. Ltd. China. Fraxetin, was purchased from Macklin Biochemical Co. Ltd. China. Nitroblue tetrazolium and HEPES were purchased from Aladdin Industrial Co. Ltd. China. Flavin mononucleotide was purchased from Sigma-Aldrich Co. Ltd. USA. Yeast extract, tryptone were purchased from Sangon Biotech Co. Ltd. China.

2.2. Strains and growth conditions

Shewanella oneidensis MR-1 (ATCC-700550) were maintained as freezer stocks. Mutants *S. oneidensis* MR-1 strains in which *mtr* pathway genes (Δ*cymA*, Δ*mtrA*, *and* Δ*mtrC/omcA*) were generated previously (Zhu et al., 2022). Mutants *S. oneidensis* MR-1 Δ*dmsA/dmsB* (SO_1047/SO_1430) were constructed for this study following established protocols (Gao et al., 2009), and the relevant plasmid information is provided in Supplementary Materials. Before the start of each experiment strains were precultured in 100 mL of lysogeny broth medium.

2.3. Electrochemical measurements

Cyclic voltammetry (CV) measurements were conducted using a CHI832D potentiostat (CHI Instruments, Shanghai, China) with a scan rate of 50 mV/s using a platinum plate counter electrode and an Ag/AgCl reference. 1 mM solution of fraxetin was prepared by dissolving in ultrapure water at 60 °C and stored at 4 °C, whereas 1 mM solutions of FMN was prepared by dissolving in ultrapure water and stored at 4 °C in the dark. The electrolyte consisted of 20 mM HEPES and 5 g/L NaCl, with the pH adjusted to 7.00 using NaOH. ESs were added to a final concentration of 10 μM. For CV under anoxic conditions, the electrolyte was continuously purged with N_2 for 30 min prior to scanning. For oxic conditions, the electrolyte was purged with oxygen for 30 min to reach dissolved oxygen saturation before scanning. Data shown are generally from the third of three scans.

Solutions of FMN and fraxetin were prepared at a final concentration of 100 μM in electrolyte and transferred into serum bottles. The solutions were purged with N_2 for 30 min and then placed in an anoxic chamber (95% N_2, 5% H_2, with a palladium catalyst) with the caps open for 24 h to remove residual oxygen. Subsequently, *S. oneidensis* MR-1 cells were added inside the glove box and incubated for 6 h for reduction (as indicated by the color change of FMN from yellow to colorless). The cultures were then centrifuged and filtered to remove cells, yielding reduced FMN and fraxetin solutions. Chronoamperometric measurements under anoxic conditions were conducted in an anaerobic chamber. A potential of +0.4 V (vs. Ag/AgCl) was applied, and after 10 min of baseline stabilization, reduced FMN or fraxetin was introduced into the system. Chronoamperometric measurements under oxic conditions were performed under continuous oxygen purging.

2.4. Measurement of superoxide anion

A 1 mM nitroblue tetrazolium (NBT) solution was prepared in HEPES buffer (pH 7.00), removed oxygen by continuous N_2 purging for 30 min, and then placed in an anoxic chamber with the caps open for 6 h to remove residual oxygen. 2.5 mL of reduced fraxetin or reduced FMN was mixed with 2.5 mL of NBT solution in sealable glass vials inside an

anoxic chamber. For the anoxic condition, the vials were sealed in an anoxic chamber and reacted for 5 min before measurement. For the oxic condition, oxygen was purged into the sealed vials for 5 min prior to measurement. The sealed glass vials were directly placed in a UV–visible spectrophotometer equipped with the appropriate module (Genesys 30, Thermo Fisher, USA), and absorbance at 560 nm was recorded to determine superoxide anion production (Kim et al., 2022).

2.5. Density functional theory (DFT) calculations

The theoretical calculations were performed using the Gaussian 16 program with ωB97X-D (Chai & Head-Gordon, 2008) functional. Geometries were optimized in the water solvent using the 6-6-311++G (d, p) basis set, and the single-point energy refinements were further performed with 6-311++G (d, p) basis set. Harmonic frequency analysis was performed to verify the optimized geometries to be minima (no imaginary frequency).

For frontier molecular orbitals: The solvent effect was evaluated using the solution model based on density solvation model. The frontier molecular orbitals analysis was performed through the Multiwfn 3.8 software together with the VMD program.

For thermodynamic parameters: The single-point energy calculations were performed on the optimized geometries at ωB97X-D/6-311++G (d, p) theoretical level (Krishnan et al., 1980). Approximate solvent effects of water were taken into consideration based on the continuum solvation model in optimization and the single-point energy calculations (Marenich et al., 2009). The initial structures of $H_9O_4^+$ and H_8O_4 are obtained from the references (Temelso et al., 2011). The reduction potentials are calculated as Eqs. (1)–(3):

$$O_2 + 2H_9O_4^+ + 2e^- \rightarrow H_2O_2 + 2H_8O_4 \quad (1)$$

$$\text{oxidized FMN} + 2H_9O_4^+ + 2e^- \rightarrow \text{reduced FMNH}_2 + 2H_8O_4 \quad (2)$$

$$\text{oxidized fraxetin} + 2H_9O_4^+ + 2e^- \rightarrow \text{reduced Fraxetin} + 2H_8O_4 \quad (3)$$

2.6. Construction of three-electrode systems

Two types of electrolytes were used for culturing *S. oneidensis* MR-1 in three-electrode systems. A basal electrolyte, designed to minimize the influence of biomass variation, contained 20 mM HEPES, 0.6 g/L K_2HPO_4, 0.3 g/L NH_4Cl, 5 g/L NaCl, and 10 mM sodium lactate as the electron donor, adjusted to pH 7.00. A nutrient electrolyte, supplemented with 0.1 g/L casamino acids, was used for toxicity assays and transcriptomic analyses. The growth of *S. oneidensis* MR-1 in these two electrolytes (see Supplementary Materials), demonstrates that *S. oneidensis* MR-1 only grew in nutrient electrolyte with casamino acids.

Three-electrode systems were assembled with a total volume of 150 mL electrolyte. Both the working and counter electrodes consisted of graphite felt (2 × 2 cm), while an Ag/AgCl (saturated KCl) electrode served as the reference. A constant potential of + 0.2 V (vs. Ag/AgCl) was applied using a CHI1000C/1030C potentiostat (CHI Instruments, Shanghai, China). The three-electrode systems were equipped with a sterile aeration system delivering gas at 40 mL/min, and a magnetic stirrer was used to maintain mixing during operation. For N_2–air switching experiments, three-electrode systems were filled with 150 mL basal electrolyte supplemented with 10 μM of the indicated ES at the start. To initiate experiments, pre-cultured *S. oneidensis* MR-1 cells were harvested by centrifugation at 6000*g* for 5 min and resuspended in 10 g/L NaCl solution. Washed cells were then inoculated into each treatment at a final OD_{600} of 0.1 (typically 1.5 mL cell suspension into 150 mL electrolyte, ~1.48×10^8 CFU/mL). Systems were initially operated under continuous N_2 purging until a stable current was established, after which the purge gas was switched to air at the same flow rate. For mutants, all mutants were introduced into the three-electrode systems after 7–8 h of air purging, at which point the baseline current had stabilized and the medium was saturated with dissolved oxygen. The final OD_{600} of inoculated cells was adjusted to 0.1.

To investigate fraxetin mediated EET, three-electrode systems were operated with nutrient electrolyte supplemented with 10 μM fraxetin at the start, and inoculated with 1% (v/v) Washed *S. oneidensis* MR-1cells. CV was performed with a scan range from –0.6 to + 0.6 V and a scan rate of 50 mV/s. Electrochemical impedance spectroscopy (EIS) as conducted using an Autolab electrochemical potentiostat, with the working electrode potential poised at 0.2 V vs. Ag/AgCl and a sinusoidal perturbation of 10 mV applied over a frequency range from 100 kHz to 100 mHz. EIS data were fitted using ZView2 software.

2.7. Transcriptomic analysis

Triplicate samples of *S. oneidensis* MR-1 electrode biofilms supplemented with fraxetin, along with triplicate biofilm samples without supplementation, were harvested after 16 h of three-electrode system operation (marked as the experimental group and the control group, respectively). Total RNA was isolated using the Trizol Reagent (Invitrogen Life Technologies). Quality and integrity were determined using a NanoDrop spectrophotometer (Thermo Scientific). Zymo-Seq RiboFree Total RNA Library Kit was used to remove rRNA from total RNA. Random oligonucleotides and SuperScript III were used to synthesize the first strand cDNA. Second strand cDNA synthesis was subsequently performed using DNA Polymerase I and RNase H (Strand-specific RNA-seq: Then use RNaseH to degrade the RNA strand, and in the DNA polymerase I system, use dNTP with dUTP instead of dTTP as raw material to synthesize the second strand of cDNA). Remaining overhangs were converted into blunt ends via exonuclease/polymerase activities and the enzymes were removed. After adenylation of the 3′ ends of the DNA fragments, Illumina PE adapter oligonucleotides were ligated to prepare for hybridization. To select cDNA fragments of the preferred 400–500 bp in length, the library fragments were purified using the AMPure XP system (Beckman Coulter, Beverly, CA, USA). DNA fragments with ligated adaptor molecules on both ends were selectively enriched using Illumina PCR Primer Cocktail in a 15 cycle PCR reaction. Products were purified (AMPure XP system) and quantified using the Agilent high sensitivity DNA assay on a Bioanalyzer 2100 system (Agilent). The sequencing library was then sequenced on NovaSeq 6000 platform (Illumina) by Shanghai Personal Biotechnology Cp. Ltd.

2.8. Statistical analysis

Statistical analyses were performed in Prism 9.5.1(733) for windows (GraphPad Software). For comparisons between two groups, a two-tailed Student's *t*-test was used to assess significance. For comparisons among three or more groups, one-way ANOVA followed by Tukey's post-hoc test was performed. Significance levels were denoted as follows: ns (not significant, $P > 0.05$), * $P \leq 0.05$, ** $P \leq 0.01$, *** $P \leq 0.001$).

3. Results and discussion

3.1. The electron exchange capacity of ESs under oxic conditions

To assess whether oxygen interferes with the electron exchange capacity of ESs, cyclic voltammetry (CV) conducted under both oxic and anoxic conditions showed that the oxidation peak of FMN was almost completely absent in the presence of oxygen (Fig. 1a), suggested that reduced FMN may react with oxygen, thereby preventing its reoxidation at the electrode surface. In contrast, fraxetin maintained consistent redox peaks under both conditions (Fig. 1b). Under anoxic conditions, supplementation with reduced FMN in three-electrode systems produced pronounced oxidative current (see Supplementary Materials). However, the oxidative current was completely abolished under saturated dissolved oxygen (DO) conditions, suggesting that oxygen prevented the electrode from capturing the electrons carried by reduced

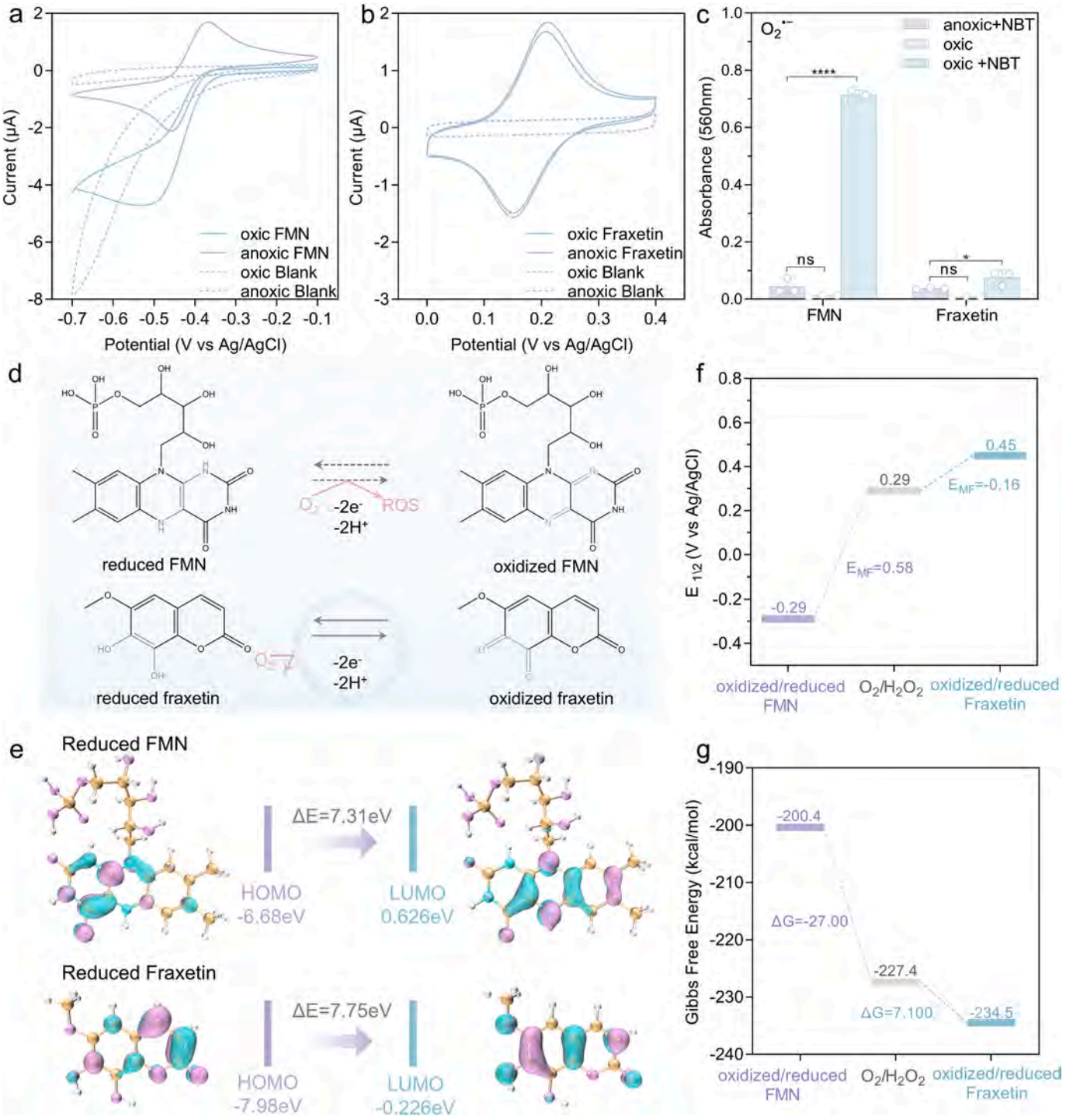

Fig. 1. Electrochemical performance of different ESs under oxic conditions. (a) CV of FMN at identical sterile glassy carbon electrodes under anoxic or saturated DO conditions. (b) CV of fraxetin at identical sterile glassy carbon electrodes under anoxic or saturated DO conditions. (c) Absorbance changes of NBTsolution at 560 nm under different reaction conditions. Reaction condition of experimental group: 100 μM electron shuttle and 100 μM NBT in a HEPES buffer (100 mM, pH 7.00) under anoxic or oxic conditions. (d) Structures of oxidized and reduced FMN and fraxetin. (e) Calculated molecular orbital for reduced FMN and reduced fraxetin. (f) Calculated redox potential for FMN, O_2 and fraxetin. (g) Gibbs free-energy diagrams for FMN, O_2 and fraxetin. All the data are presented as averages ± SD (n = 3).

FMN. In contrast, reduced fraxetin generated comparable oxidative current under both anoxic and saturated DO conditions, implying that the electrons carried by reduced fraxetin could still be captured by the electrode in the presence of oxygen (see Supplementary Materials). To assess potential reactive oxygen species formation, nitroblue tetrazolium (NBT) was employed as a superoxide detection probe (Kim et al., 2022) (see Supplementary Materials). Neither reduced FMN nor reduced fraxetin produced superoxide under anoxic conditions (Fig. 1c). However, under saturated DO conditions, reduced FMN reacted with oxygen to generate detectable levels of superoxide, while reduced fraxetin exhibited no detectable superoxide formation (Fig. 1c). In summary, these results indicate that the electrons carried by the amide group of reduced FMN were readily captured by oxygen, thus limiting electron transfer to other acceptors. In contrast, the phenolic hydroxyl group of reduced fraxetin remained chemically stable, and its electrons were not easily captured by oxygen (Fig. 1d).

The distinct responses of FMN and fraxetin under oxic conditions prompted us to perform DFT calculations, focusing on frontier molecular orbitals and thermodynamic parameters. According to frontier orbital theory, the highest occupied molecular orbital (HOMO) energy is a key indicator of electron donating propensity, as a higher HOMO corresponds to easier oxidation and a lower ionization potential (Akbari et al., 2024). Meanwhile, the energy gap between the HOMO and the lowest unoccupied molecular orbital (LUMO) reflects molecular stability and reactivity, with smaller gaps generally indicating higher reactivity (Su et al., 2018). The results showed that the HOMO energy level of reduced FMN (−6.68 eV) was higher than that of reduced fraxetin (−7.89 eV), indicating that reduced FMN possesses stronger reducing ability and is more prone to donate electrons (Fig. 1e). Moreover, the energy gap of reduced FMN (7.31 eV) was smaller than that of reduced fraxetin (7.75 eV), suggesting that reduced FMN is more chemically reactive (Fig. 1e). Together, these frontier orbital results explained the greater susceptibility of reduced FMN to oxygen oxidation compared with reduced fraxetin.

Thermodynamic analyses further support these conclusions. The calculated Gibbs free energy change for the reaction between reduced FMN and oxygen is –27.00 kcal/mol, indicating that the oxidation of reduced FMN by oxygen is thermodynamically favorable, whereas the corresponding value for reduced fraxetin was +7.10 kcal/mol, indicating the oxidation of reduced fraxetin by oxygen thermodynamically unfavorable (Fig. 1f). Similarly, the reaction electromotive force is +0.58 eV for FMN and −0.16 eV for fraxetin, further confirming that spontaneous redox reactions with oxygen were feasible for reduced FMN but not for reduced fraxetin (Fig. 1g). These results demonstrated that FMN is intrinsically vulnerable to oxygen attack and rapidly loses its electron exchange capacity under oxic conditions, whereas fraxetin resists oxygen oxidation as an oxygen-tolerant ES due to its high thermodynamic stability. Notably, the oxidation of organic molecules at a glassy carbon electrode mainly proceeds via an outer-sphere electron transfer mechanism, in which no chemical bonding to the electrode is required and electrons tunnel through molecular orbitals, enabling efficient oxidation even with a modest thermodynamic driving force (Bard & Faulkner, 2001). In contrast, oxygen is a triplet molecule, and its homogeneous electron transfer with organic substrates is strongly hindered by weak orbital coupling and a high activation barrier (Ingold & Pratt, 2014). Therefore, under oxic conditions, reduced fraxetin can still preferentially donate electrons to an electrode with a lower oxidation potential than oxygen, thus functioning as an electron shuttle.

3.2. Oxygen impacts ESs mediated EET in S. Oneidensis MR-1

Building on the distinct thermodynamic stability of FMN and fraxetin described above, we next examined whether these differences would be manifested in the EET of *S. oneidensis* MR-1. To this end, *S. oneidensis* MR-1 was inoculated into three electrode systems supplemented with either FMN or fraxetin, and oxidation current dynamics were monitored under bottom aerating at 40 mL/min, with the gas switched from N_2 to air. With FMN, the system produced a stable oxidation current of 3.05 ± 0.09 mA·cm^{-2}·OD$^{1}_{600}$ under continuous N_2 purging, but upon switching to air (DO: ~7.0 mg/L), decreased rapidly to 1.02 ± 0.55 mA·cm^{-2}·OD$_{600}$

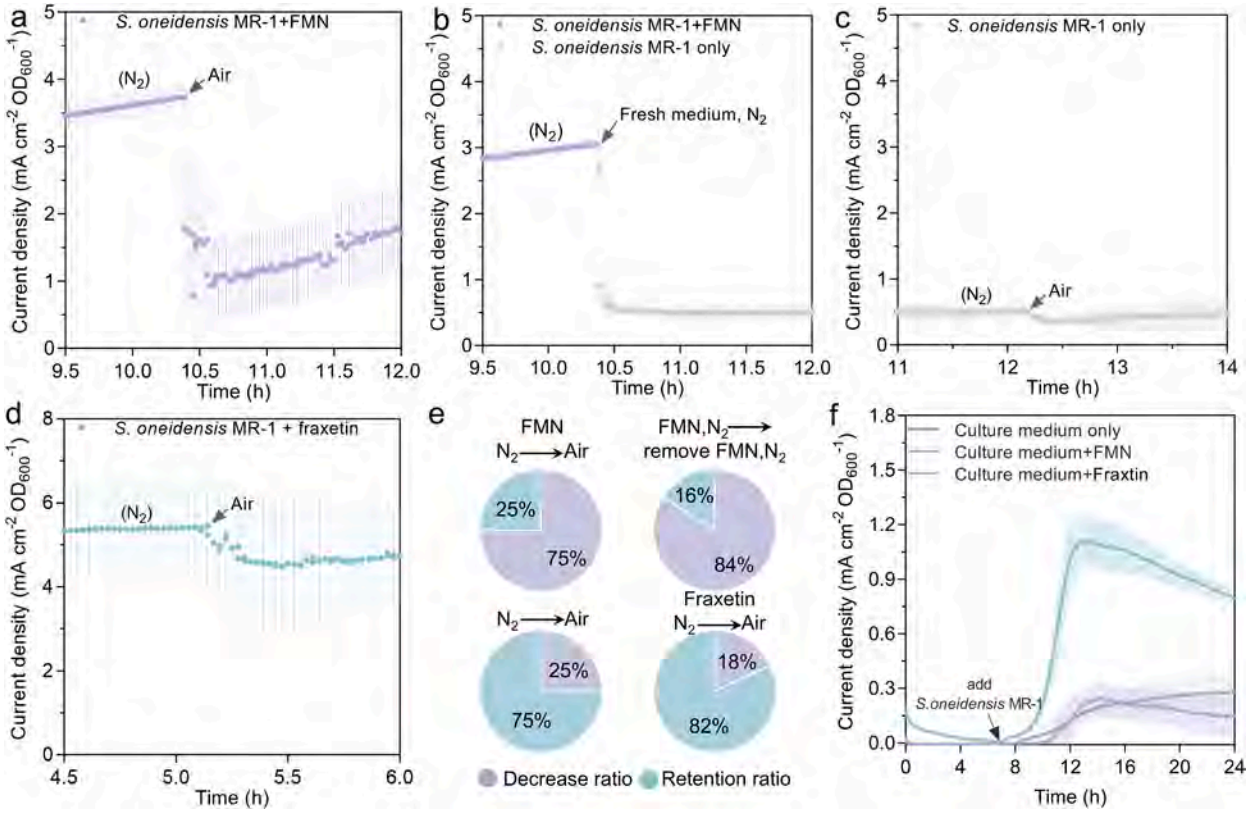

Fig. 2. Effects of oxygen intrusion on ESs mediated EET. (a) Oxidation current generated by an established *S. oneidensis* MR-1 biofilm with 10 μM FMN under continuous N_2 flow (40 mL/min, the same below). The arrow indicated the point where N_2 was switched to continuous air flow. Data points were recorded at 1 min intervals. (b) Oxidation current was generated by a biofilm with 10 μM FMN under continuous N_2 flow; at the arrow, the medium was replaced with fresh medium lacking FMN (cells retained in the supernatant) while N_2 flow was maintained. (c) Oxidation current was generated by a biofilm under continuous N_2 flow; the arrow indicated the switch from N_2 to continuous air flow. (d) Oxidation current was generated by a biofilm with 10 μM fraxetin under continuous N_2 flow; the arrow indicated the switch from N_2 to continuous air flow. (e) Relative current changes before and after gas switching under different conditions. Decrease rate (purple): the proportion of current decrease after the state switch. Retention rate (green): the proportion of current retained after the state switch. (f) Oxidation current generated by *S. oneidensis* MR-1 under oxic conditions without ESs or with 10 μM ESs. All the data are presented as averages ± SD (n = 3).

^{1} (Fig. 2a), accompanied by a color change of the medium from pale yellow (reduced FMN) to bright yellow (oxidized FMN) (see Supplementary Materials). When the FMN-containing medium was replaced with fresh FMN-free medium and cells were reintroduced under N_2, the current rapidly decreased from 3.73 ± 0.20 mA cm^{-2} OD_{600}^{-1} to 0.52 ± 0.11 mA·cm^{-2}·OD_{600}^{-1} (see Supplementary Materials). Notably, once a new stable current of 0.44 ± 0.08 mA·cm^{-2}·OD_{600}^{-1} was established in this FMN-free system, switching from N_2 to air (DO: ~7.0 mg/L) caused the current to decrease only to 0.36 ± 0.07 mA·cm^{-2}·OD_{600}^{-1} (Fig. 2c). In addition, systems containing *S. oneidensis* MR-1 and fraxetin maintained stable oxidation currents of 5.45 ± 1.49 mA·cm^{-2}·OD_{600}^{-1} under N_2, and upon switching to air (DO: ~7.0 mg/L), the current decreased only gradually, stabilizing at 4.58 ± 1.37 mA·cm^{-2}·OD_{600}^{-1} of the initial value (Fig. 2d). These results indicated that the distinct thermodynamic stability of FMN and fraxetin resulted in different responses of mediating EET in *S. oneidensis* MR-1 under oxygen infiltration conditions.

To gain a deeper understanding of these phenomena, we conducted an integrated analysis of the observations described above. Both oxygen exposure and FMN removal caused sharp current decreases, with reductions of 75% and 84%, respectively (Fig. 2e), indicating that oxygen primarily inhibited FMN-mediated EET. In contrast, oxygen had only a modest impact on FMN-free systems, where the current decreased by only 25%, suggesting that the observed current decreases were mainly due to partial diversion of electrons toward aerobic respiration rather than a direct termination of EET. Fraxetin, however, behaved similarly to the FMN-free control (Fig. 2e), showing only a minor current decrease of 18%, demonstrating that fraxetin mediated EET was largely insensitive to oxygen. Besides, added 10 μM FMN failed to enhance current generation, showing no significant difference from *S. oneidensis* MR-1 only, whereas added 10 μM fraxetin significantly increased the current by ~3.93-fold (Fig. 2h). In contrast, under anoxic conditions, both fraxetin and FMN enhanced the current generated by *S. oneidensis* MR-1, with no significant difference in the magnitude of the current (see Supplementary Materials). These results further suggested that fraxetin mediated EET in *S. oneidensis* MR-1 was stable under oxic conditions. Although FMN at 100 μM promoted EET under oxic conditions (see Supplementary Materials), this did not change the fact that FMN mediated EET remained sensitive to oxygen, and such a concentration far exceeds environmentally relevant levels (~2 μM) (Light et al., 2018), limiting its ecological relevance. In summary, these results demonstrated that FMN readily lost its functionality under oxic conditions, whereas fraxetin remained chemically stable and mediated efficient EET in *S. oneidensis* MR-1, highlighting thermodynamic stability as a key determinant of ESs functionality under oxygen infiltration environments.

3.3. Fraxetin mediated EET under oxic conditions

To elucidate why fraxetin mediated EET by *S. oneidensis* MR-1 remains stable under oxygen diffusion, we conducted comparative

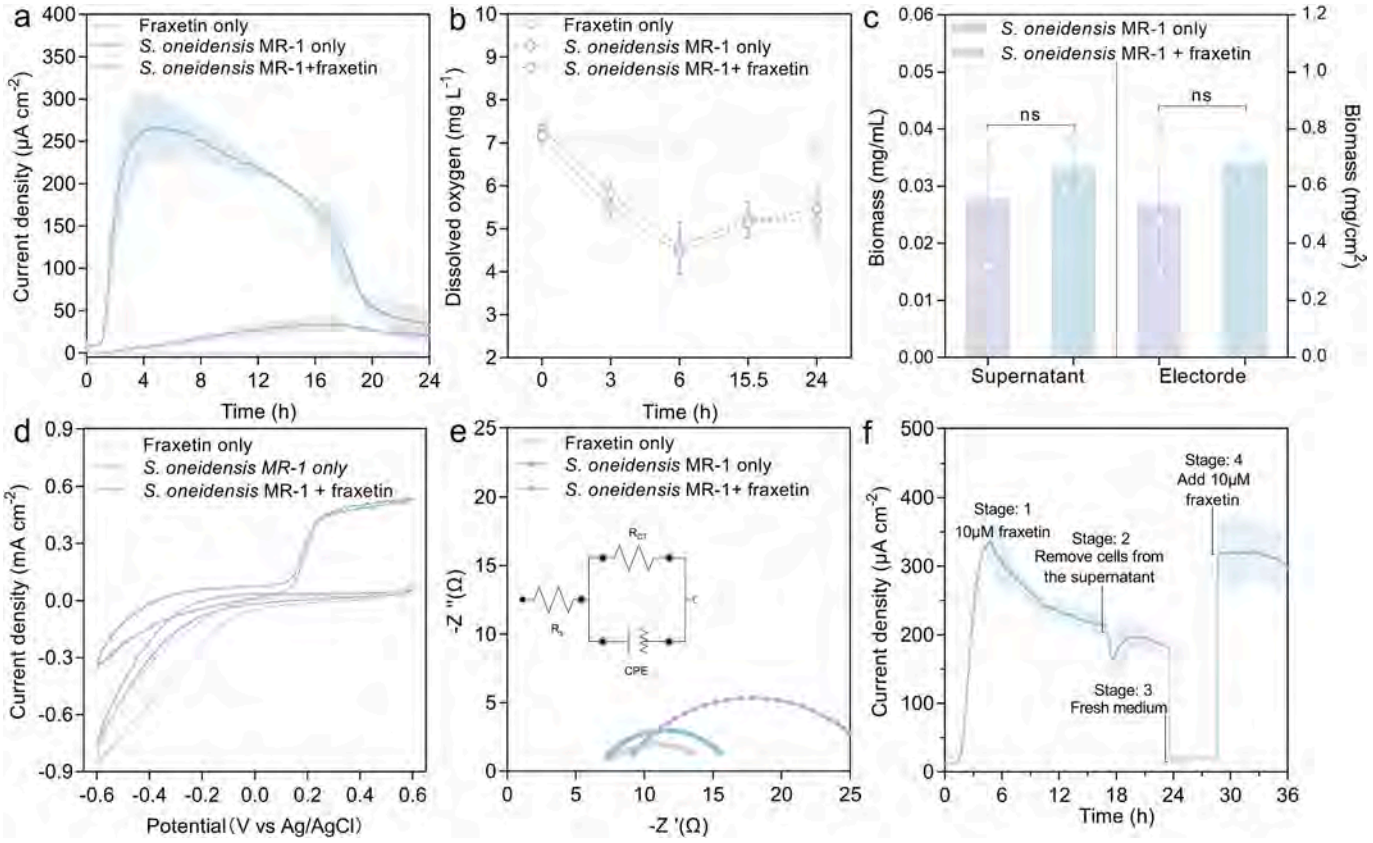

Fig. 3. Fraxetin mediates EET in *S. oneidensis* MR-1 under oxic conditions. (a) Oxidation current generated by *S. oneidensis* MR-1 under continuous air flow (40 mL/min) in the presence of fraxetin, absence of fraxetin, and with fraxetin only (no cells). (b) Dissolved oxygen concentration dynamics corresponding to the experimental conditions in Fig. 3a. (c) Quantification of biomass on electrodes and in the supernatant at 15.5 h in the presence or absence of fraxetin, measured by coomassie brilliant blue protein assay. (d) CV (scans rate:1 mV/s) of *S. oneidensis* MR-1 at 15.5 h under oxic conditions: with fraxetin, without fraxetin, and with fraxetin only (no cells). (e) Electrochemical impedance spectroscopy analysis of *S. oneidensis* MR-1 at 15.5 h under oxic conditions: presence of fraxetin, absence of fraxetin, and with fraxetin only (no cells). (f) Changes in oxidation current of *S. oneidensis* MR-1 under oxic conditions across different treatments. Stage 1: Biofilm cultivation of *S. oneidensis* MR-1 and fraxetin. Stage 2: Retention of biofilm and fraxetin, with cells from the supernatant removed by centrifugation. Stage 3: Replacement of medium with a new medium free of fraxetin, while retaining the *S. oneidensis* MR-1 electrode biofilm. Stage 4: Addition of 10 μM fraxetin. All the data are presented as averages ± SD (n = 3).

analyses in a three-electrode system that supports microbial growth under oxic conditions. Fraxetin concentrations above 10 μM significantly inhibited bacterial growth, whereas oxidation current increased in a dose-dependent manner and plateaued at 10 μM (see Supplementary Materials). The maximum current density generated by *S. oneidensis* MR-1 in the presence of 10 μM fraxetin was approximately 8-fold higher than that of *S. oneidensis* MR-1 only (Fig. 3a). In contrast, fraxetin only produced negligible currents, confirming that the enhancement required metabolically active cells. DO remained stable at ~7.0 mg/L in the fraxetin only, while inoculated systems showed moderate DO depletion due to aerobic respiration, yet levels consistently remained above 4.0 mg/L (Fig. 3b), indicating sustained oxygen availability. Quantification of biomass on the electrodes and in the supernatant (Fig. 3c) revealed no significant difference between the with or without fraxetin, indicating that the enhanced current density was not due to increased cell growth. Together, these results supported that fraxetin promotes EET in *S. oneidensis* MR-1 under oxic conditions.

To further evaluate the mechanism by which fraxetin promotes EET in *S. oneidensis* MR-1 under oxic conditions, we conducted electrochemical analyses. Cyclic voltammetry (CV) revealed that biofilms formed by *S. oneidensis* MR-1 with fraxetin produced significantly higher current than the biofilm without fraxetin (Fig. 3d). Notably, the increased current coincided with the redox potential of fraxetin, further supporting its involvement in facilitating biofilm electron transfer under oxic conditions. Electrochemical impedance spectroscopy (EIS) further demonstrated that the charge transfer resistance was lowest in the fraxetin only system (due to the absence of biofilm), highest in the biofilm without fraxetin, and markedly reduced when fraxetin was present, indicating that fraxetin facilitates interfacial electron transfer between cells and the electrode (Fig. 3e). Medium replacement experiments showed that removing supernatant cells from the three-electrode system under oxic conditions initially caused a current drop, which

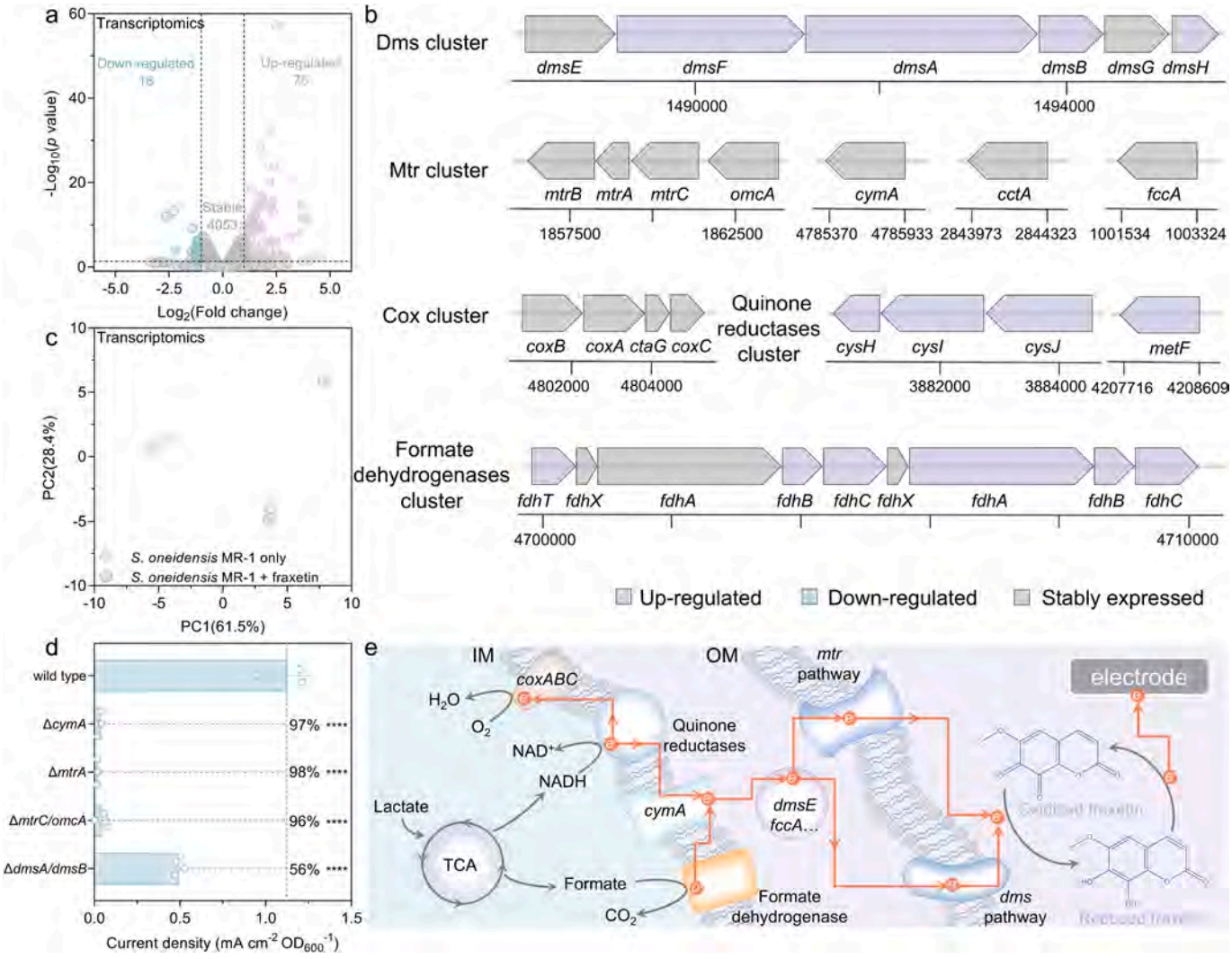

Fig. 4. Transcriptome analysis of fraxetin mediated EET by *S. oneidensis* MR-1 under oxic conditions. (a) Volcano plot demonstrating detected genes from electrode biofilm with and without fraxetin under oxic conditions. The differentially expressed genes (*S. oneidensis* MR-1 + fraxetin/ *S. oneidensis* MR-1 only) were determined by fold change ≥ 2 and P < 0.05. (b) Expression of gene clusters of interest. The *dms* cluster includes genes for *c*-type cytochromes (*dmsABEFGH*). The *mtr* cluster contains genes for *c*-type cytochromes (*cymA, mtrABC, omcA, cctA* and *fccA*). The cox cluster includes genes for *c*-type cytochromes oxidases of the electron transport chain (*coxABC* and *ctaG*). The quinone reductases cluster contains genes for 5,10-methylenetetrahydrofolate reductase (*metF*), sulfite reductase (NADPH) flavoprotein subunit (*cysJ*), sulfite reductase (NADPH) siroheme FeS subunit (*cysI*), and phosphoadenylyl-sulfate reductase thioredoxin-dependent (*cysH*). The formate dehydrogenases cluster contains genes for formate dehydrogenase (*fdhABCTX*). (c) The principal component analysis (PCA) of differentially expressed genes from from electrode biofilm with and without fraxetin under oxic conditions. (d) Maximum current density achieved from chronoamperometry experiments with *S. oneidensis* MR-1 and representative EET mutants. (e) Proposed pathway of EET mediated by fraxetin in *S. oneidensis* MR-1 under oxic conditions. All the data are presented as averages ± SD (n = 3).

quickly recovered (Fig. 3f), indicating that indicating that fraxetin mediated current density was primarily contributed by the biofilm. When the supernatant was replaced with fresh medium lacking fraxetin, the current density decreased by ~90% and re-adding fraxetin rapidly restored the current density (Fig. 3f), further confirming that fraxetin directly mediated interfacial electron transfer between *S. oneidensis* MR-1 biofilm and the electrodes.

Cyclic voltammetry under saturated dissolved oxygen conditions revealed that the peak current of fraxetin showed a linear relationship with both the scan rates and the square root of the scan rates, suggesting that its redox process under oxic conditions is influenced by both adsorption and diffusion (see Supplementary Materials). Diffusion plays a critical role in long-range electron transfer, such as between microbial cells and solid-state electron acceptors (Zheng et al., 2020). Additionally, stability tests of fraxetin showed that after 1000 cycles of cyclic voltammetry, there were no significant shifts in its redox peaks (Fig. S7c), confirming that fraxetin is a stable ES under oxic conditions. In summary, these results suggested that fraxetin can efficiently mediate EET in *S. oneidensis* MR-1 even under oxic conditions, indicating that fraxetin mediated EET is minimally compromised by oxygen diffusion.

3.4. Shewanella response to fraxetin mediated EET under oxic conditions

Since fraxetin mediated EET in *S. oneidensis* MR-1 remains stable under oxygen diffusion, we further sought to elucidate the biological impact of fraxetin on *S. oneidensis* MR-1 under oxic conditions. To this end, we performed transcriptomic analysis on electrode biofilms obtained from three-electrode systems with or without fraxetin. In total, 4145 genes from *S. oneidensis* MR-1 were detected, of which 4053 were stably expressed (fold change < 2) under both conditions (Fig. 4a). The Mtr pathway, the critical route for EET in *S. oneidensis* MR-1 (Shi et al., 2016), exhibited similar expression levels of its genes in both systems, including the inner membrane *c*-type cytochrome (*cymA*), periplasmic *c*-type cytochrome (*cctA* and *fccA*), and outer membrane *c*-type cytochromes (*mtrABC* and *omcA*), indicating that the Mtr pathway genes were stably expressed under oxic conditions and remained unaffected by fraxetin (Fig. 4b and Supplementary Materials). Likewise, *c*-type cytochrome genes related to aerobic respiration (*coxABC* and *ctaG*) (Zhou et al., 2013) were all stably expressed in both with and without fraxetin (Fig. 4b and Supplementary Materials). Together, these results indicate that fraxetin does not interfere with aerobic respiration and the Mtr pathway mediated EET process under oxic conditions.

Principal component analysis revealed that the first two components accounted for 89.9% of the variance, and the samples clustered distinctly, indicating that the significant gene expression difference between with and without fraxetin (Fig. 4c). Among the detected differential expression genes, 76 genes were significantly upregulated (fold change > 2) in the presence of fraxetin. Notably, the outer membrane *c*-type cytochrome genes of the Dms pathway (*dmsABFH*), which is homologous to the Mtr pathway, were significantly upregulated (Gralnick et al., 2006), suggesting that fraxetin may facilitate electron transfer from the Dms pathway to the electrode under oxic conditions (Fig. 4b and Supplementary Materials). In addition, four quinone reductases (Kundu et al., 2025): phosphoadenylyl-sulfate reductase thioredoxin-dependent (*cysH*), sulfite reductase siroheme FeS subunit (*cysI*), sulfite reductase flavoprotein subunit (*cysJ*), and 5,10-methylenetetrahydrofolate reductase (*metF*), which are involved in catalyzing NAD(P)H oxidation to $NAD(P)^+$ and releasing electrons, were significantly upregulated (Fig. 4b and Supplementary Materials). Moreover, the formate dehydrogenase genes (*fdhABCTX*) were also significantly upregulated (Fig. 4b and Supplementary Materials). Formate dehydrogenase is known to oxidize formate generated from lactate metabolism in the tricarboxylic acid (TCA) cycle of *S. oneidensis* MR-1, transferring the released electrons to the *c*-type cytochrome protein CymA, which subsequently transfers electrons through the Mtr and Dms pathways to the extracellular environment (Luo et al., 2016; Mordkovich et al., 2013). We further found that antioxidant processes related genes *met* and *cys* clusters (Imlay, 2013) were significantly upregulated (Fig. 4b and Supplementary Materials), indicating that fraxetin does not promote electron transfer in *S. oneidensis* MR-1 under oxic conditions by enhancing antioxidant activity. Based on these findings, we hypothesize that fraxetin mediated EET under oxic conditions is facilitated by enhanced electron transfer from the Dms pathway to the electrode, with the electrons derived primarily from quinone reductases and formate dehydrogenase in the inner membrane.

To validate the above hypothesis, we examined *S. oneidensis* MR-1 together with mutants deficient in the Mtr or Dms pathways. Unexpectedly, the maximum current density produced by the Δ*cymA*, Δ*mtrA*, and Δ*mtrC/omcA* mutants under oxic conditions with fraxetin decreased by more than 96% compared to the wild type, whereas the Δ*dmsA/dmsB* mutant showed only a 56% decrease (Fig. 4d). These findings indicate that both the Mtr and Dms pathways are involved in fraxetin mediated EET under oxic conditions, and that defects in the Mtr pathway may impair the function of the Dms pathway. Nonetheless, the role of the Dms pathway cannot be overlooked, as its absence resulted in a ~44% reduction in current density. Therefore, we propose that the mechanism of fraxetin-mediated EET in *S. oneidensis* MR-1 under oxic conditions involves facilitating electron transfer between the Mtr and Dms pathways and the electrode, stimulating quinone reductases and formate dehydrogenase to generate more electrons that are delivered to *cymA* and subsequently relayed via periplasmic *c*-type cytochromes to both pathways, thereby supporting rapid electron transfer (Fig. 4e).

4. Conclusion

In conclusion, this work establishes a generalizable strategy to address the long-standing challenge of oxygen infiltration in BESs by leveraging antioxidants as ESs. Guided by electrochemical characterization and density functional theory calculations, we reveal that the high thermodynamic stability of fraxetin as an oxygen-tolerant ES under oxic conditions. Unlike the conventional flavin mononucleotide, which is readily oxidized by oxygen and prone to generate reactive oxygen species, the natural antioxidant fraxetin exhibits high stability, thereby maintaining efficient interfacial electron transfer between *S. oneidensis* MR-1 and electrodes even under dissolved oxygen levels exceeding 4 mg L^{-1}. Importantly, fraxetin-mediated EET not only enhanced the maximum current density but also significantly reduced the decrease in current output under oxygen infiltration. Our findings highlight oxygen-tolerant ESs as a robust and versatile avenue to maintain efficient interfacial electron transfer in bio-electrochemical systems under oxygen infiltration. This bio-inspired concept provides a new framework for the rational selection of ESs, paving the way toward more efficient, stable, and practical BESs applications in energy generation, environmental remediation, biosensors, and bioelectronics under actual environments.

CRediT authorship contribution statement

Wei Chen: Writing – original draft, Methodology, Formal analysis, Data curation, Conceptualization. **Rui Bai:** Methodology, Formal analysis, Data curation. **Biyi Zhao:** Validation, Formal analysis, Data curation. **Xudong Zhou:** Writing – review & editing, Formal analysis. **Feng Zhao:** Writing – review & editing, Methodology, Conceptualization. **Yong Xiao:** Writing – review & editing, Project administration, Methodology, Funding acquisition, Conceptualization.

Declaration of competing interest

The authors declare that they have no known competing financial interests or personal relationships that could have appeared to influence the work reported in this paper.

Acknowledgements

This work was supported by the National Natural Science Foundation of China (22276183), Institute of Urban Environment, Chinese Academy of Sciences (IUE-JBGS-202212), and the Youth Innovation Promotion Association, Chinese Academy of Sciences (Y2022082).

Appendix A. Supplementary data

Supplementary data to this article can be found online at https://doi.org/10.1016/j.biortech.2026.134250.

Data availability

Data will be made available on request.

References

Aiyer, K., Doyle, L.E., 2022. Capturing the signal of weak electricigens: a worthy endeavour. Trends Biotechnol. 40 (5), 564–575.

Akbari, Z., Stagno, C., Iraci, N., Efferth, T., Omer, E.A., Piperno, A., Montazerozohori, M., Feizi-Dehnayebi, M., Micale, N. 2024. Biological evaluation, DFT, MEP, HOMO-LUMO analysis and ensemble docking studies of Zn(II) complexes of bidentate and tetradentate Schiff base ligands as antileukemia agents. *J. Mol. Struct.*, **1301**.

Amirdehi, M.A., Khodaparastasgarabad, N., Landari, H., Zarabadi, M.P., Miled, A., Greener, J., 2020. A high-performance membraneless microfluidic microbial fuel cell for stable, long-term benchtop operation under strong flow. ChemElectroChem 7 (10), 2227–2235.

Atkinson, J.T., Su, L., Zhang, X., Bennett, G.N., Silberg, J.J., Ajo-Franklin, C.M., 2022. Real-time bioelectronic sensing of environmental contaminants. Nature 611 (7936), 548-+.

Bard, A.J., Faulkner, L.R., 2001. *Electrochemical Methods: Fundamentals and Applications*. John Wiley & Sons, New York.

Cao, B., Zhao, Z., Peng, L., Shiu, H.-Y., Ding, M., Song, F., Guan, X., Lee, C.K., Huang, J., Zhu, D., Fu, X., Wong, G.C.L., Liu, C., Nealson, K., Weiss, P.S., Duan, X., Huang, Y., 2021. Silver nanoparticles boost charge-extraction efficiency in *Shewanella* microbial fuel cells. Science 373 (6561), 1336-+.

Chai, J.-D., Head-Gordon, M., 2008. Long-range corrected hybrid density functionals with damped atom-atom dispersion corrections. PCCP 10 (44), 6615–6620.

Choi, S., 2022. Electrogenic bacteria promise new opportunities for powering, sensing, and synthesizing. Small 18 (18).

Choi, S., Chae, J., 2013. Optimal biofilm formation and power generation in a micro-sized microbial fuel cell (MFC). Sens. Actuator A-Phys. 195, 206–212.

Gao, H., Yang, Z.K., Barua, S., Reed, S.B., Romine, M.F., Nealson, K.H., Fredrickson, J.K., Tiedje, J.M., Zhou, J., 2009. Reduction of nitrate in *Shewanella oneidensis* depends on atypical NAP and NRF systems with NapB as a preferred electron transport protein from CymA to NapA. ISME J. 3 (8), 966–976.

Gralnick, J.A., Vali, H., Lies, D.P., Newman, D.K., 2006. Extracellular respiration of dimethyl sulfoxide by Shewanella oneidensis strain MR-1. PNAS 103 (12), 4669–4674.

Harnisch, F., Deutzmann, J.S., Boto, S.T., Rosenbaum, M.A., 2024. Microbial electrosynthesis: opportunities for microbial pure cultures. Trends Biotechnol. 42 (8), 1035–1047.

Imlay, J.A., 2013. The molecular mechanisms and physiological consequences of oxidative stress: lessons from a model bacterium. Nat. Rev. Microbiol. 11 (7), 443–454.

Ingold, K.U., Pratt, D.A., 2014. Advances in radical-trapping antioxidant chemistry in the 21st century: a kinetics and mechanisms perspective. Chem. Rev. 114 (18), 9022–9046.

Khan, M.T., Duncan, S.H., Stams, A.J.M., van Dijl, J.M., Flint, H.J., Harmsen, H.J.M., 2012. The gut anaerobe *Faecalibacterium prausnitzii* uses an extracellular electron shuttle to grow at oxic-anoxic interphases. ISME J. 6 (8), 1578–1585.

Kim, J., Nguyen, T.V.T., Kim, Y.H., Hollmann, F., Park, C.B., 2022. Lignin as a multifunctional photocatalyst for solar-powered biocatalytic oxyfunctionalization of C–H bonds. Nat. Synth. 1 (3), 217–226.

Krishnan, R., Binkley, J.S., Seeger, R., Pople, J.A., 1980. Self-consistent molecular-orbital methods.20. basis set for correlated wave-functions. J. Chem. Phys. 72 (1), 650–654.

Kundu, B.B., Krishnan, J., Szubin, R., Patel, A., Palsson, B.O., Zielinski, D.C., Ajo-Franklin, C.M., 2025. Extracellular respiration is a latent energy metabolism in *Escherichia coli*. Cell 188 (11).

Li, C., Yi, K., Hu, S., Yang, W., 2023. Cathodic biofouling control by microbial separators in air-breathing microbial fuel cells. Env Sci. Ecotechnol. 15.

Li, S., Zuo, X., Carpenter, M.D., Verduzco, R., Ajo-Franklin, C.M., 2025. Microbial bioelectronic sensors for environmental monitoring. Nat. Rev. Bioeng. 3 (1), 30–49.

Li, T., Yang, X.-L., Chen, Q.-L., Song, H.-L., He, Z., Yang, Y.-L., 2020. Enhanced performance of microbial fuel cells with electron mediators from anthraquinone/polyphenol-abundant herbal plants. ACS Sustain. Chem. Eng. 8 (30), 11263–11275.

Light, S.H., Su, L., Rivera-Lugo, R., Cornejo, J.A., Louie, A., Iavarone, A.T., Ajo-Franklin, C.M., Portnoy, D.A., 2018. A flavin-based extracellular electron transfer mechanism in diverse Gram-positive bacteria. Nature 562 (7725), 140.

Lin, X., Yang, F., You, L.-X., Wang, H., Zhao, F., 2021. Liposoluble quinone promotes the reduction of hydrophobic mineral and extracellular electron transfer of *Shewanella oneidensis* MR-1. Innov.-Amsterd. 2 (2), 100104.

Logan, B.E., Rossi, R., Ragab, A.A., Saikaly, P.E., 2019. Electroactive microorganisms in bioelectrochemical systems. Nat. Rev. Microbiol. 17 (5), 307–319.

Luo, S., Guo, W., Nealson, K.H., Feng, X., He, Z., 2016. ^{13}C pathway analysis for the role of formate in electricity generation by *Shewanella oneidensis* MR-1 using lactate in microbial fuel cells. Sci. Rep. 6.

Ma, J., Yu, W., Li, X., Chen, S., Wu, B., Wang, J., Chen, B., Chu, C., 2025. Quinones stimulate reactive oxygen species production from zero-valent iron over centimeter distances. Water Res. 274.

Marenich, A.V., Cramer, C.J., Truhlar, D.G., 2009. Universal solvation model based on solute electron density and on a continuum model of the solvent defined by the bulk dielectric constant and atomic surface tensions. J. Phys. Chem. B 113 (18), 6378–6396.

Marsili, E., Baron, D.B., Shikhare, I.D., Coursolle, D., Gralnick, J.A., Bond, D.R., 2008. *Shewanella* secretes flavins that mediate extracellular electron transfer. PNAS 105 (10), 3968–3973.

McRose, D.L., Li, J., Newman, D.K., 2023. The chemical ecology of coumarins and phenazines affects iron acquisition by *Pseudomonads*. PNAS 120 (14), e2217951120.

Medina, M.E., Iuga, C., Alvarez-Idaboy, J.R., 2014. Antioxidant activity of fraxetin and its regeneration in aqueous media. a density functional theory study. RSC Adv. 4 (95), 52920–52932.

Mittler, R., Zandalinas, S.I., Fichman, Y., Van Breusegem, F., 2022. Reactive oxygen species signalling in plant stress responses. Nat. Rev. Mol. Cell Biol. 23 (10), 663–679.

Mordkovich, N.N., Voeikova, T.A., Novikova, L.M., Smirnov, I.A., Il'in, V.K., Soldatov, P. E., Tyurin-Kuz'min, A.Y., Smolenskaya, T.S., Veiko, V.P., Shakulov, R.S., Debabov, V. G., 2013. Effect of NAD^+-dependent formate dehydrogenase on anaerobic respiration of *Shewanella oneidensis* MR-1. Microbiology 82 (4), 404–409.

Okamoto, A., Hashimoto, K., Nealson, K.H., Nakamura, R., 2013. Rate enhancement of bacterial extracellular electron transport involves bound flavin semiquinones. PNAS 110 (19), 7856–7861.

Price-Whelan, A., Dietrich, L.E.P., Newman, D.K., 2006. Rethinking 'secondary' metabolism: physiological roles for phenazine antibiotics. Nat. Chem. Biol. 2 (2), 71–78.

Shahidi, F., Ambigaipalan, P., 2015. Phenolics and polyphenolics in foods, beverages and spices: Antioxidant activity and health effects - a review. J. Funct. Food. 18, 820–897.

Shi, L., Dong, H., Reguera, G., Beyenal, H., Lu, A., Liu, J., Yu, H.Q., Fredrickson, J.K., 2016. Extracellular electron transfer mechanisms between microorganisms and minerals. Nat. Rev. Microbiol. 14 (10), 651–662.

Su, Y., Li, Y., Ganguly, R., Kinjo, R., 2018. Engineering the frontier orbitals of a diazadiborinine for facile activation of H_2, NH_3, and an isonitrile. Angew. Chem.-Int. Edit. 57 (26), 7846–7849.

Temelso, B., Archer, K.A., Shields, G.C., 2011. Benchmark structures and binding energies of small water clusters with anharmonicity corrections. Chem. A Eur. J. 115 (43), 12034–12046.

Wang, C., Wei, X., Wang, Y., Wu, C., Jiao, P., Jiang, Z., Liu, S., Ma, Y., Guan, S., 2025. Metabolomics and transcriptomic analysis revealed the response mechanism of maize to saline-alkali stress. Plant Biotechnol. J.

Xiao, Y., Chen, G., Chen, Z., Bai, R., Zhao, B., Tian, X., Wu, Y., Zhou, X., Zhao, F., 2021. Interspecific competition by non-exoelectrogenic *Citrobacter freundii* An1 boosts bioelectricity generation of exoelectrogenic *Shewanella oneidensis* MR-1. Biosens. Bioelectron. 194, 113614.

Xiao, Y., Zhang, E., Zhang, J., Dai, Y., Yang, Z., Christensen, H.E.M., Ulstrup, J., Zhao, F., 2017. Extracellular polymeric substances are transient media for microbial extracellular electron transfer. Sci. Adv. 3 (7).

Xie, Y., Ersan, S., Guan, X., Wang, J., Sha, J., Xu, S., Wohlschlegel, J.A., Park, J.O., Liu, C., 2023. Unexpected metabolic rewiring of CO_2 fixation in H_2-mediated materials-biology hybrids. PNAS 120 (42).

Yan, W., Guo, Y., Xiao, Y., Wang, S., Ding, R., Jiang, J., Gang, H., Wang, H., Yang, J., Zhao, F., 2018. The changes of bacterial communities and antibiotic resistance genes in microbial fuel cells during long-term oxytetracycline processing. Water Res. 142, 105–114.

Yang, C., Aslan, H., Zhang, P., Zhu, S., Xiao, Y., Chen, L., Khan, N., Boesen, T., Wang, Y., Liu, Y., Wang, L., Sun, Y., Feng, Y., Besenbacher, F., Zhao, F., Yu, M., 2020. Carbon dots-fed *Shewanella oneidensis* MR-1 for bioelectricity enhancement. Nat. Commun. 11 (1).

Yang, J., Cheng, S., Li, P., Huang, H., Cen, K., 2019. Sensitivity to oxygen in microbial electrochemical systems biofilms. iScience 13, 163.

Yoon, J.Y., Ahn, Y., Sehröder, U., 2018. Parylene C-coated PDMS-based microfluidic microbial fuel cells with low oxygen permeability. J. Power Sources 398, 209–214.

Zhang, J., Li, F., Liu, D., Liu, Q., Song, H., 2024a. Engineering extracellular electron transfer pathways of electroactive microorganisms by synthetic biology for energy and chemicals production. Chem. Soc. Rev. 53 (3), 1375–1446.

Zhang, L., Zhang, Y., Liu, Y., Wang, S., Lee, C.K., Huang, Y., Duan, X., 2024b. High power density redox-mediated *Shewanella* microbial flow fuel cells. Nat. Commun. 15 (1).

Zheng, Y., Wang, H., Liu, Y., Zhu, B., Li, J., Yang, Y., Qin, W., Chen, L., Wu, X., Chistoserdova, L., Zhao, F., 2020. Methane-dependent mineral reduction by aerobic methanotrophs under hypoxia. Environ. Sci. Technol. Lett. 7 (8), 606–612.
Zhou, G., Yin, J., Chen, H., Hua, Y., Sun, L., Gao, H., 2013. Combined effect of loss of the caa3 oxidase and Crp regulation drives *Shewanella* to thrive in redox-stratified environments. ISME J. 7 (9), 1752–1763.
Zhu, T., Cheng, Z., Yu, S., Li, W., Liu, D., Yu, H., 2022. Unexpected role of electron-transfer hub in direct degradation of pollutants by exoelectrogenic bacteria. Environ. Microbiol. 24 (4), 1838–1848.